Received: 21 April 2021 | Revised: 25 May 2021 | Accepted: 1 June 2021

DOI: 10.1002/jrs.6174

RESEARCH ARTICLE

Journal of RAMAN SPECTROSCOPY WILEY

Shedding light onto the spectra of lime—Part 2: Raman spectra of Ca and Mg carbonates and the role of *d*-block element luminescence

Thomas Schmid[1,2] | **Ronja Kraft**[1] | **Petra Dariz**[2,3]

[1]Department 1 – Analytical Chemistry; Reference Materials, Bundesanstalt für Materialforschung und -prüfung (BAM), Berlin, Germany

[2]School of Analytical Sciences Adlershof (SALSA), Humboldt-Universität zu Berlin, Berlin, Germany

[3]Institute Materiality in Art and Culture, Bern University of the Arts, Bern University of Applied Sciences, Bern, Switzerland

Correspondence
Thomas Schmid, Bundesanstalt für Materialforschung und -prüfung (BAM), Richard-Willstätter-Str. 11, 12489 Berlin, Germany.
Email: thomas.schmid@bam.de

Funding information
Deutsche Forschungsgemeinschaft, Grant/Award Number: DFG GSC 1013 SALSA

Abstract

We previously described the observation of a characteristic narrowband red luminescence emission of burnt lime (CaO), whose reason was unknown so far. This study presents Raman spectra of $Mg_5(CO_3)_4(OH)_2{\cdot}4H_2O$, $Mg_5(CO_3)_4(OH)_2$, $MgCO_3$, $CaMgCO_3$ and $CaCO_3$ (in limestone powder) as well as luminescence spectra of their calcination products. Comparison of the latter revealed MgO:Cr^{3+} as the source of the red lime luminescence in all studied samples, containing magnesium oxide as major component, minor component or trace. Spectral characteristics and theoretical background of the luminescence emission of *d*-block elements integrated in crystal lattices are discussed with the aim of sharpening the awareness for this effect in the Raman community and promoting its application in materials analysis. The latter is demonstrated by the Raman microspectroscopic imaging of the distributions of both Raman-active and Raman-inactive phases in clinker remnants in a 19th-century meso Portland cement mortar sample, which contain relatively high amounts of free lime detected in the form of both luminescing CaO and Raman-scattering $Ca(OH)_2$, owing to exposure of the surface of the thin section to humid air. A combination of light and Raman spectroscopy revealed a calcium–magnesium–iron sulphide phase, indicating sulphurous raw materials and/or solid fuels employed in the calcination process, which in contrast to previously described morphologies of sulphides in cement clinker form extensive greenish black layers on free lime crystals.

KEYWORDS

calcium carbonates, luminescence, magnesium carbonates, meso Portland cement, MgO:Cr^{3+}

Thomas Schmid and Petra Dariz contributed equally to this manuscript.

1 | INTRODUCTION

In the predecessor paper to this article, we described a red luminescence emission consisting of several sharp lines (thus, in some other studies confused with Raman bands), which within the phases of the lime cycle was assigned to burnt lime (calcium oxide, CaO), because the effect was lost upon slaking to calcium hydroxide and not restored during carbonation to calcium carbonate.[1] Due to its specificity, this luminescence effect was employed for mapping the distribution of Raman-inactive free lime CaO in the microspectroscopic imaging of a 19th-century Portland cement mortar sample,[2] but the reason for the emission was not known so far. A literature survey yields foreign element ions, fluorescing point defects (F centres) and radical ions (e.g., $O^{-\bullet}$) in the crystal lattice as possible reasons.[1]

Because often, rare earth (*f*-block) elements are mentioned in the discussion of luminescence in inorganic phases, we would like to emphasise the possibility of *d*-block element ions in a crystal field as potential reason and give the Raman community a better understanding of the according theoretical background. In our predecessor study, rare earth element ions were considered unlikely as fluorophores, because of the reproducibility of the observed spectral pattern requiring that always the same of these easily interchangeable elements would have to be present in CaO.[1] A narrowband luminescence emission caused by Cr^{3+} ions integrated in the crystal lattice of MgO—close chemical relative of CaO—was described by Otto Deutschbein in 1932,[3] followed by studies investigating either the sharp central band and features closely nearby[4–6] or the full spectral pattern including satellite bands around the central feature.[7–9] Anastasia Chopelas described the theoretical background of this effect in detail.[9]

A Cr^{3+} ion replacing a Mg^{2+} in the cubic crystal lattice of MgO is octahedrally coordinated by six O^{2-} ions. The two *d* orbitals of Cr^{3+} with lobes along the octahedral axes ($3d_{x^2-y^2}$ and $3d_{z^2}$) interact with the orbitals of the oxygen ions and are raised, whereas the other three with lobes between the axes ($3d_{xy}$, $3d_{xz}$ and $3d_{yz}$) are lowered in energy. According to ligand field theory, the resulting upper two levels are termed e_g and the lower three t_{2g}. The electron configuration of the $^4A_{2g}$ ground state of Cr^{3+} in an octahedral field is t_{2g}^3 with three unpaired spins, that is, a multiplicity of 4. Because the ligand field of MgO results in a high energy difference between the e_g and t_{2g} levels, the energy needed for spin pairing is lower than for transition of an electron into an e_g level ('low spin'). Thus, the first excited state ^2E_g has the same t_{2g}^3 electron configuration but reduced multiplicity of 2 due to spin pairing. The equilibrium bond distances in the ground and first excited state are almost the same, according to the Franck–Condon principle favouring absorptions and emissions between the ground vibrational states of both electronic levels. This situation is inherent to complexes with small distances between the central Cr^{3+} and surrounding O^{2-}, further than MgO:Cr^{3+} including Al_2O_3:Cr^{3+} (ruby or sapphire), $Mg_3Al_2(SiO_4)_3$:Cr^{3+} (pyrope), $Y_3Al_5O_{12}$:Cr^{3+} (yttrium aluminium garnet, YAG), $MgAl_2O_4$:Cr^{3+} (spinel[9] and $(Mg,Fe,Al)_6(AlSi_3O_{10})(OH)_8$:$Cr^{3+}$ (clinochlore),[10] leading to well-defined transitions and sharp bands usually in the red spectral range, therefore termed R lines.[9] Weaker interactions between central ion and ligands, for example, in Mg_2SiO_4:Cr^{3+} (forsterite) and $CaMgSi_2O_6$:Cr^{3+} (diopside), favour the transition of an electron into another orbital over spin reversal. Compared with the $^4A_{2g}$ ground state, the first excited state $^4T_{2g}$ is characterised by the changed electron configuration t_{2g}^2 e_g^1, same multiplicity ('high spin') and significantly different bond distance resulting in the excitation into an (almost) continuum of levels and a spectrally broad emission,[9] that is, a fluorescence more familiar to Raman spectroscopists, because known as unwanted 'background' and baseline raise. The same applies to emission from the higher excited state $^4T_{2g}$ of MgO:Cr^{3+}, which is observed as broad band centred at approximately 16 150 cm^{-1}.[11]

Substitution of two Mg^{2+} by two Cr^{3+} ions generates an additional 2+ charge, which is compensated by one vacancy on a magnesium site. Variations in amount and spatial proximity of vacancies cause different types of distortion of the Cr^{3+} centres and thus small shifts of energy levels, which are the reasons for so-called N lines ('Nebenlinien'), appearing Stokes shifted (or red shifted, respectively) within approximately 5 nm from the R line.[3–6,9] Bands appearing symmetrically within approximately ±500 cm^{-1} on both sides of the R line are due to transitions to or from vibrational levels of the involved electronic states.[7–9]

This article presents Raman spectra of magnesium and Ca–Mg carbonates (the spectrum of $Mg_5(CO_3)_4(OH)_2$ has not been described in the literature so far) and luminescence spectra of MgO and CaO. Comparison of the latter enables the elucidation of the source of the previously described red lime luminescence.[1] A survey of basic principles of this effect is aimed to sharpen the awareness and provide strategies for the identification and assignment of narrowband fluorescence effects in the Raman community, where mainly the ruby luminescence emitted by Al_2O_3:Cr^{3+} seems to be relatively widely known. Perhaps, the present study can similarly bridge

the fields of Raman scattering and luminescence emission like the pioneering study on ruby by Rappal S. Krishnan.[12] Zofia Kaszowska et al. described broadband and narrowband fluorescence emission from different mineral phases relevant in lime-based building and conservation materials (see literature[13] and references cited therein), and the complex field of architectural heritage with a focus on mortar components seems particularly suited for gaining deeper insight by combining Raman with luminescence spectroscopy. Therefore, we demonstrate the evaluation of the red lime luminescence emission for mapping the distributions of both Raman-active and Raman-inactive phases within the same experiment, enabling a better understanding of the raw material mixture and calcination conditions of a 19th-century Portland cement binder produced in a shaft kiln.

2 | EXPERIMENTAL

2.1 | Samples

Hydromagnesite and calcium carbonate were purchased from Carl Roth GmbH + Co. KG (Karlsruhe, Germany) and Merck KGaA (Emsure®, Darmstadt, Germany), respectively, whereas a limestone powder (Kalksteinwerk Mendenbach GmbH, Germany) was taken from a collection of Bundesanstalt für Materialforschung und -prüfung (BAM, Department 7, Berlin, Germany), and samples of dolomite (Garbenteich near Gießen, Hesse, Germany) and magnesite (Styria, Austria) were provided by Museum für Naturkunde (Berlin, Germany). Rock samples were powdered in the laboratories of Department 7 at BAM.

For triggering the red lime luminescence emission in an analytical grade calcium carbonate sample (Emsure®, Merck), 5 g of the $CaCO_3$ powder were mixed with 25-mg chromium(III) oxide (reference material, Speciality Products and homogenised in a ball mill for 10 min prior to calcination at 1100°C (see result in Figure S5).

A sample was taken from a cast building ornament originating from the residential building Florastrasse 54 in Zurich (Switzerland), raised in 1875. The cement stone was embedded in epoxy resin under vacuum for the preparation of polished thin sections with the standard thickness of 30 μm known from petrographic analyses by polarised light microscopy (see Figures 5 and S8).

2.2 | Calcination

The samples were calcined either in a heating stage (TS-1500 with T96-LinkPad controller, Linkam, Tadworth, UK) placed on the sample scanning stage of the Raman microscope or in a laboratory furnace (LT 9/13/P320, Nabertherm, Lilienthal, Germany). The heating stage is equipped with a firmly installed corundum crucible (3-mm diameter and 7-mm height, taking up to 10- to 20-mg powder of the materials used in this study), whose bottom opening for transmitted light microscopy was closed with a submillimetre thin sapphire disk. The crucible was closed with a corundum lid and heated with the highest possible rate of 200 K min^{-1}. After reaching the according set point, the temperature was kept constant for 10 min (see Figure 4) or 1 h (see Figure 1), and the Raman measurements were performed in the crucible after cooling to room temperature.

For calcination in the laboratory furnace, 5-g sample powder was filled into a corundum crucible (3.5-cm diameter and 5-cm height). The furnace was heated with the highest possible rate of approximately 30 K min^{-1}, and the set point temperature was held for 4 h. The samples were cooled and stored in a desiccator. For Raman measurements, sample aliquots were transferred onto conventional microscope glass slides by using a spatula.

2.3 | Raman microscope and measurement conditions

The Raman measurements were performed by using a LabRam HR800 Raman microscopy system (Horiba JobinYvon, Bensheim, Germany) coupled with a BX41 upright microscope (Olympus, Hamburg, Germany) and a 632.8-nm HeNe laser with a maximum power at the sample surface of approximately 10 mW (in all experiments except for Raman microspectroscopic imaging [see below], the unattenuated power was used). A 50×/N.A. = 0.55 long-working-distance microscope objective was employed for focusing of the laser onto the sample surface (resulting in a spot diameter of approximately 1.2 μm and a penetration depth in transparent materials of approximately 50 μm; see supporting information of Schmid et al.[14] for details) and collection of the scattered light. For acquisition of the spectra shown in Figure 1, a 300-mm^{-1} grating was employed for dispersion, yielding a spectral resolution of approximately 1.6 cm^{-1} per pixel (at 3800-cm^{-1} Raman shift) to 2.6 cm^{-1} per pixel (at 200-cm^{-1} Raman shift). For the acquisition of all other spectra, a 1800-cm^{-1} grating was used, resulting in spectral resolutions of 0.15 cm^{-1} (at 3800 cm^{-1}) to 0.34 cm^{-1} (at 200 cm^{-1}). For detection of the spectra shown in Figures 1, S1 and S4, a Peltier cooled (−60°C) Syncerity (Horiba JobinYvon) charge coupled device (CCD) camera was used, whereas for the acquisition of all other spectra, a liquid-N_2 cooled

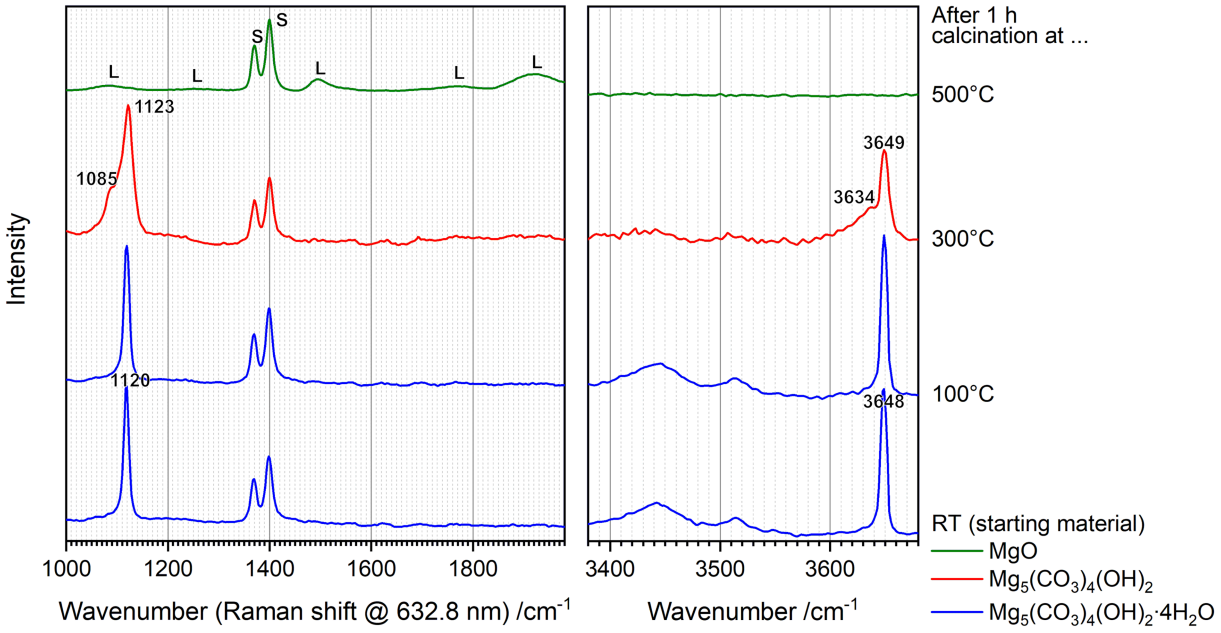

FIGURE 1 Room-temperature (RT) Raman spectrum of hydromagnesite $Mg_5(CO_3)_4(OH)_2{\cdot}4H_2O$ and according spectra acquired after calcination at 100°C, 300°C and 500°C for 1 h each. The spectra are assigned to hydromagnesite (100°C), dehydrated hydromagnesite $Mg_5(CO_3)_4(OH)_2$ (300°C) and magnesium oxide MgO (500°C). The latter consists of luminescence bands (labelled 'L'). All spectra contain the most prominent ruby luminescence ($Al_2O_3{:}Cr^{3+}$) lines emitted by the sapphire baseplate of the heating stage employed in this experiment (labelled 'S') [Colour figure can be viewed at wileyonlinelibrary.com]

(−130°C operating temperature) Symphony CCD (Horiba JobinYvon) was employed. Both CCD cameras had 1024 pixels along the spectral axis. If necessary, the typical acquisition time of 60 s was reduced while accordingly increasing the number of accumulations to avoid saturation of the detector at approximately 65 000 counts.

Unless noted otherwise, no baseline correction of spectra was performed. In figures without intensity values ('counts' or 'counts per second', respectively) on the ordinates, spectra were scaled and offset for better comparability.

Raman microspectroscopic imaging was performed with the same instrument using the same objective lens, same laser, the 300-mm^{-1} grating and the liquid-N_2 cooled CCD detector. The laser power was reduced to 2.5 mW by inserting a neutral density filter into the beam path. Raster scanning of the thin-sectional sample in x and y directions with 1.5-μm steps was controlled by the instrument's LabSpec 6 software (Horiba JobinYvon), and in each pixel of the resulting image, a Raman spectrum was acquired within 2 × 2 s (i.e., 2 accumulations of 2 s each). Thus, the Raman imaging experiments took approximately 4 h 30 min (Figure 5, 54 × 75 pixels) and 4 h 45 min (Figure S8, 65 × 65 pixels), respectively. In the Raman spectra, a linear baseline was subtracted around each marker band and peak heights were plotted in false colours in 2D diagrams by using own LabView-based software (National Instruments Corp., Austin, TX, USA) to reveal the distributions of mineral phases. The marker bands evaluated within this study were 265 cm^{-1} (Ca_2AlFeO_5), 319 cm^{-1} ((Ca,Mg,Fe)S), 356 cm^{-1} ($Ca(OH)_2$) and 858 cm^{-1} (β-Ca_2SiO_4). The baseline-corrected peak height of the R line was plotted for revealing the distribution of the red lime luminescence.

3 | RESULTS AND DISCUSSION

3.1 | Raman spectra of hydromagnesite and dehydrated hydromagnesite

Although $MgCO_3$ is ordinarily obtained by mining magnesite, the most common synthetic magnesium carbonate is hydromagnesite, which is yielded by precipitation from magnesium salt solutions. Its formula $Mg_5(CO_3)_4(OH)_2{\cdot}4H_2O$ reveals it as a basic magnesium carbonate, which according to thermal analysis, data dehydrates at 200–250°C into $Mg_5(CO_3)_4(OH)_2$. The loss of water from the hydroxide ions is followed by conversion into MgO upon release of carbon dioxide at approximately 510–550°C.[15] Figure 1 shows the room-temperature Raman spectra of hydromagnesite and its decomposition products.

The spectra assigned to hydromagnesite are in good agreement with a study by Ray L. Frost, except for the OH stretching mode at 3648 cm^{-1} missing in the literature data due to restriction of the spectral range to ≤3600 cm^{-1}.[16] Exact wavenumber positions of bands were determined by Lorentzian peak fitting[17] of data acquired with higher spectral resolution (see Figure S1; spectral resolutions are mentioned in Section 2), for example, revealing a shoulder of the OH stretching mode at 3637 cm^{-1}. In agreement with literature data on $Mg(OH)_2$, these bands are assigned to the OH^- ions of this hydrated magnesium carbonate–hydroxide, whereas the broad bands between 3400 and 3600 cm^{-1} are due to crystal water. Friedemann Freund described the according Raman mode of $Mg(OH)_2$ to appear at 3655 cm^{-1}, with six overtones detectable as absorbance peaks from the near infrared to the green spectral range, the latter at 518 nm lying within a proton conduction band above the dissociation limit of OH^- ions.[18] Due to excitation with a longer wavelength, such effects are assumed to be negligible within the present study.

The Raman spectrum of dehydrated hydromagnesite has not been described in the literature so far. It is characterised by the raise of a shoulder at 1085 cm^{-1} as well as broadening and shift of the most prominent band in the hydromagnesite spectrum from 1120 to 1123 cm^{-1} (cf. deconvolutions in Figure S1). Although the symmetric and antisymmetric stretch vibrations of crystal water are lost, the most prominent stretch vibrational mode of OH^- shifts from 3648 to 3649 cm^{-1} accompanied by the rise of a shoulder at approximately 3634 cm^{-1}. After calcination at 500°C, all Raman modes disappear, because magnesium oxide—in analogy to other compounds crystallising in the cubic halite structure[1]—is Raman inactive, and the spectrum purely consists of luminescence features: the ruby luminescence doublet related to the sapphire baseplate in the heating stage present in all spectra shown in Figure 1, and a set of peaks resembling the red lime luminescence described in our predecessor paper.[1]

3.2 | The reason for red luminescence in MgO

In the further course of the experiments, the intensities of the luminescence bands acquired at room temperature increased as a function of the previously applied calcination temperatures (see Figure S2). Figure 2 shows the example of the luminescence spectrum obtained after calcination of 5-g hydromagnesite powder at 800°C in a laboratory furnace for 4 h by measurement on a glass slide, thus avoiding the ruby luminescence bands seen in Figure 1. The spectral pattern can be fully explained by the emission of $MgO:Cr^{3+}$ as proven by the intriguing agreement with fig. 1 in Chao[7] and is in good accordance with the lime luminescence in the red range, which we previously observed in calcium oxide.[1] In the predecessor publication, we demonstrated its origin from luminescence and excluded Raman scattering as its reason by exciting spectra at different laser wavelengths. Comparison of the resulting spectra reveals Raman bands at the same wavenumbers (Raman shifts), whereas luminescence bands appear at the same emission wavelengths.[1] In Figure S3 of the present article, we demonstrate the Stokes/anti-Stokes test: luminescence bands appear only Stokes shifted from the Rayleigh line, whereas Raman bands would appear symmetrically in both the Stokes and anti-Stokes ranges.

Such symmetry is also inherent to the luminescence emission spectrum shown in Figure 2, as it is characterised by a strong and sharp central line surrounded by satellite peaks arranged at the almost same positive and negative wavenumber shifts on both sides. The abscissa is expressed in different units, of which the Raman shift or wavenumber scale at the bottom is mainly given for practical reasons, enabling a direct comparison with Raman spectra excited by the common HeNe laser wavelength of 632.8 nm. More appropriate for luminescence bands are the wavelength and absolute wavenumber scales presented on the top. We observe satellite bands Stokes shifted by approximately −411, −242, +268 and +432 cm^{-1} from the central line, appearing at 699.1 nm, 14 304 cm^{-1} (absolute wavenumbers) or 1499 cm^{-1} on the seeming Raman shift scale at 632.8 nm, respectively.

Whereas the R and N lines in Figure 2 are due to electronic transitions from the excited ^2E_g to the $^4A_{2g}$ ground state, emissions from the excited electronic state into excited vibrational levels of the ground state explain the Stokes-shifted bands, and emissions from excited vibrational levels of the excited electronic state are responsible for bands on the anti-Stokes side of the R line.[7–9] As a single wavelength is employed for excitation—that is, the laser line at 632.8 nm—the latter excited states can only be populated after thermal excitation into excited vibrational levels of the electronic ground state according to the Boltzmann distribution. Thus, the satellite bands represent a vibrational spectrum of MgO, which—similar to a Raman spectrum—consists of Stokes and anti-Stokes ranges. As different selection rules apply, this approach enables access to vibrational spectroscopy of a Raman-inactive crystal by using a Raman spectrometer. Figure 3 schematically shows energy levels and according spectral features for better explanation of the theoretical background.

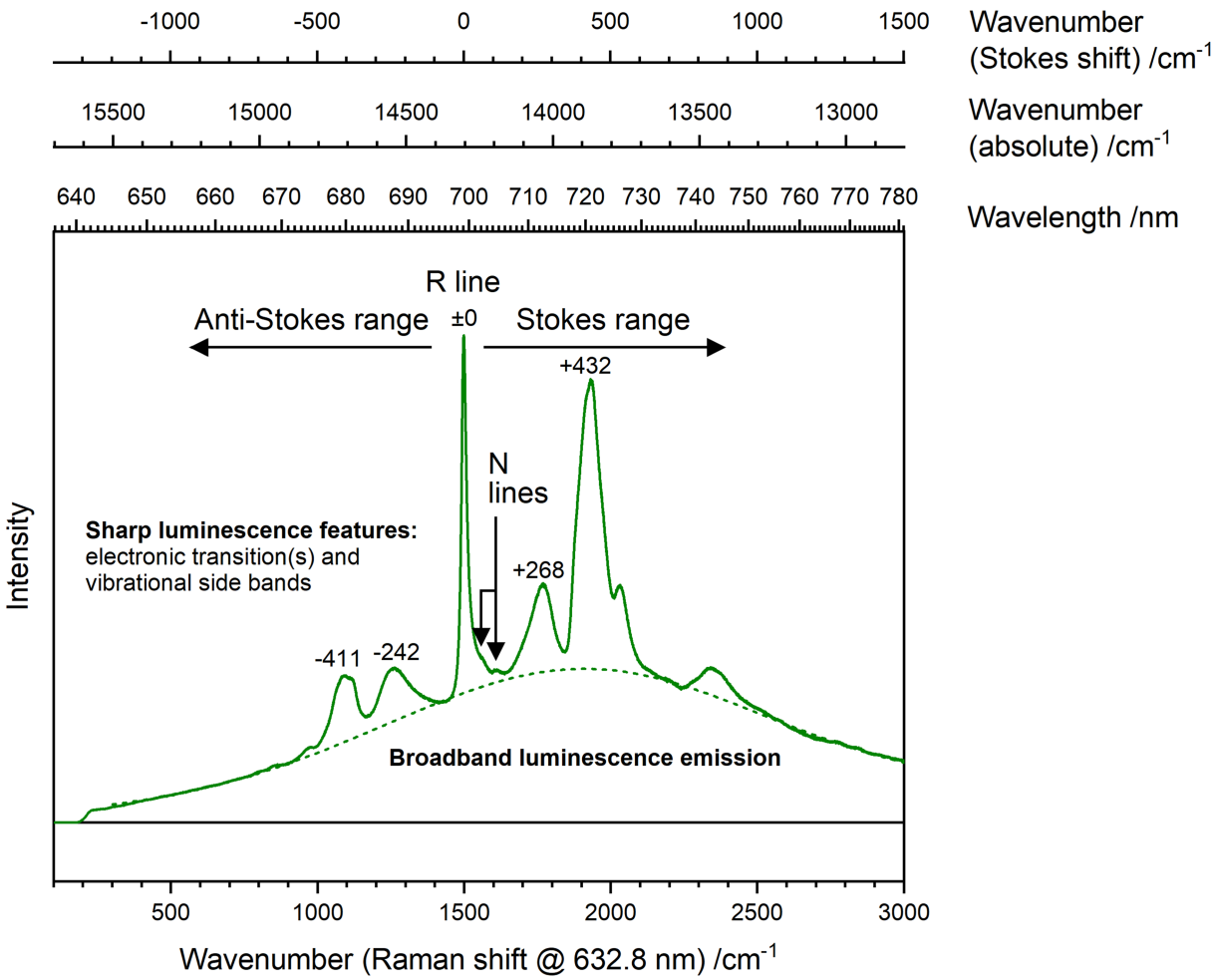

FIGURE 2 Luminescence emission spectrum of hydromagnesite calcinated into magnesium oxide at 800°C [Colour figure can be viewed at wileyonlinelibrary.com]

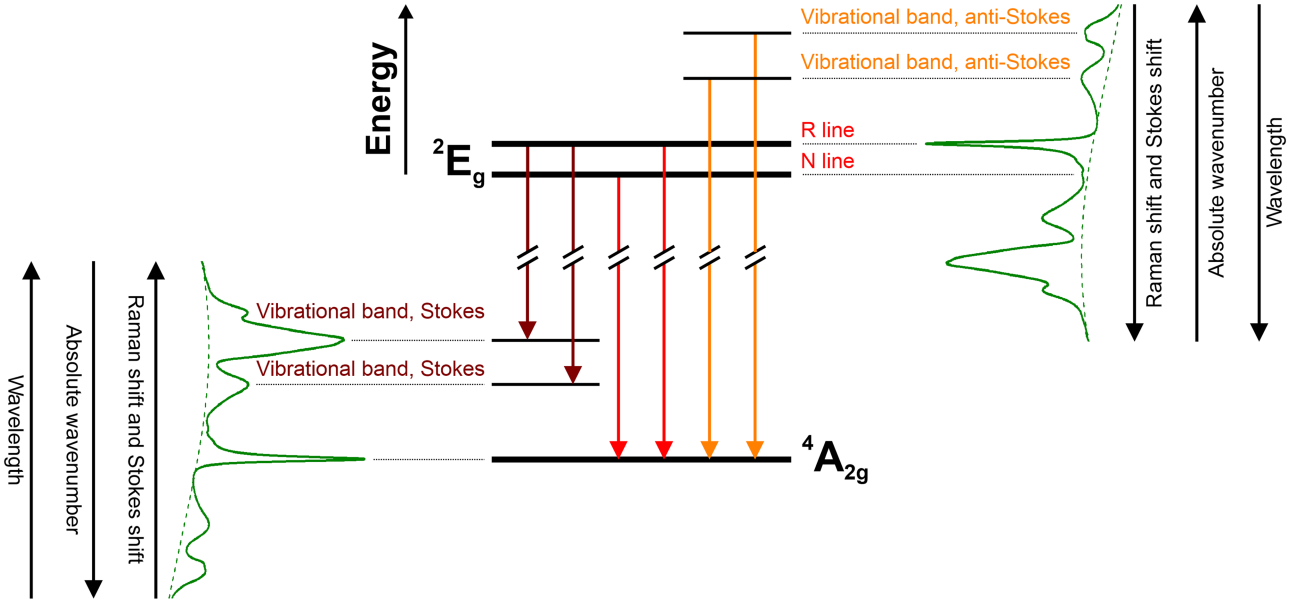

FIGURE 3 Schematical explanation of the sharp features in the red luminescence emission of MgO:Cr^{3+} [Colour figure can be viewed at wileyonlinelibrary.com]

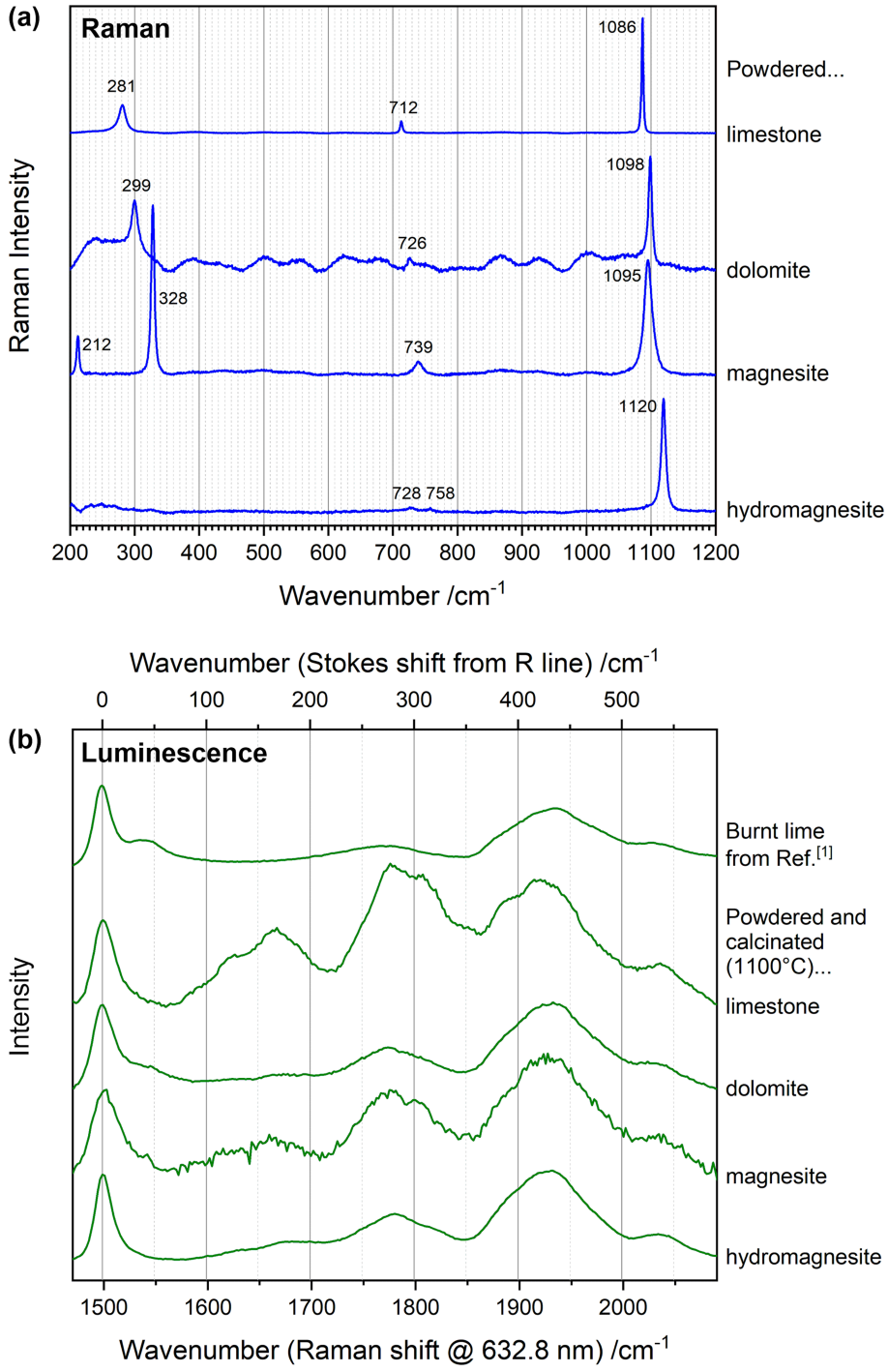

FIGURE 4 (a) Baseline-corrected Raman spectra in the range of 200 to 1200 cm^{-1} acquired in powdered hydromagnesite, magnesite, dolomite (unlabelled peaks are artefacts due to etaloning of the detector) and limestone (bands assigned to the main mineral calcite), and (b) luminescence spectra obtained after 10-min calcination of 20 mg of these mineral or stone powders at 1100°C in a heating stage (only the range Stokes shifted from the R line is shown in order to exclude the interfering R_1 and R_2 lines emitted by the sapphire baseplate of the heating stage). The luminescence spectrum of burnt lime from Schmid and Dariz[1] is shown for comparison [Colour figure can be viewed at wileyonlinelibrary.com]

The basic principle of a spectral pattern with one (or a few) sharp central electronic transition line(s) and vibrational satellite bands applies to several luminescence emissions of *d*-block element ions integrated in crystal lattices, facilitating their identification and interpretation. As another example, Figure S4 shows the well-known ruby luminescence spectrum of $Al_2O_3:Cr^{3+}$, which consists of two sharp central lines and weak vibrational side bands. There are three main differences compared with the $MgO:Cr^{3+}$ spectrum: (1) due to varied e_g–t_{2g} energy difference in the ligand field of Al_2O_3, the central feature appears blue shifted and is (2) split into an R_1 and R_2 line at approximately 692.8 nm (14 433-cm^{-1} absolute wavenumbers or 1369-cm^{-1} Stokes shifted from 632.8 nm, respectively) and 694.3 nm (14 403 or 1399 cm^{-1}, respectively) due to intrinsically stronger distortion of the octahedral coordination causing loss of degeneracy of the e_g levels,[9] and (3) the altered distances of the side bands to the R line represent the wavenumbers of the vibrational modes of Al_2O_3.

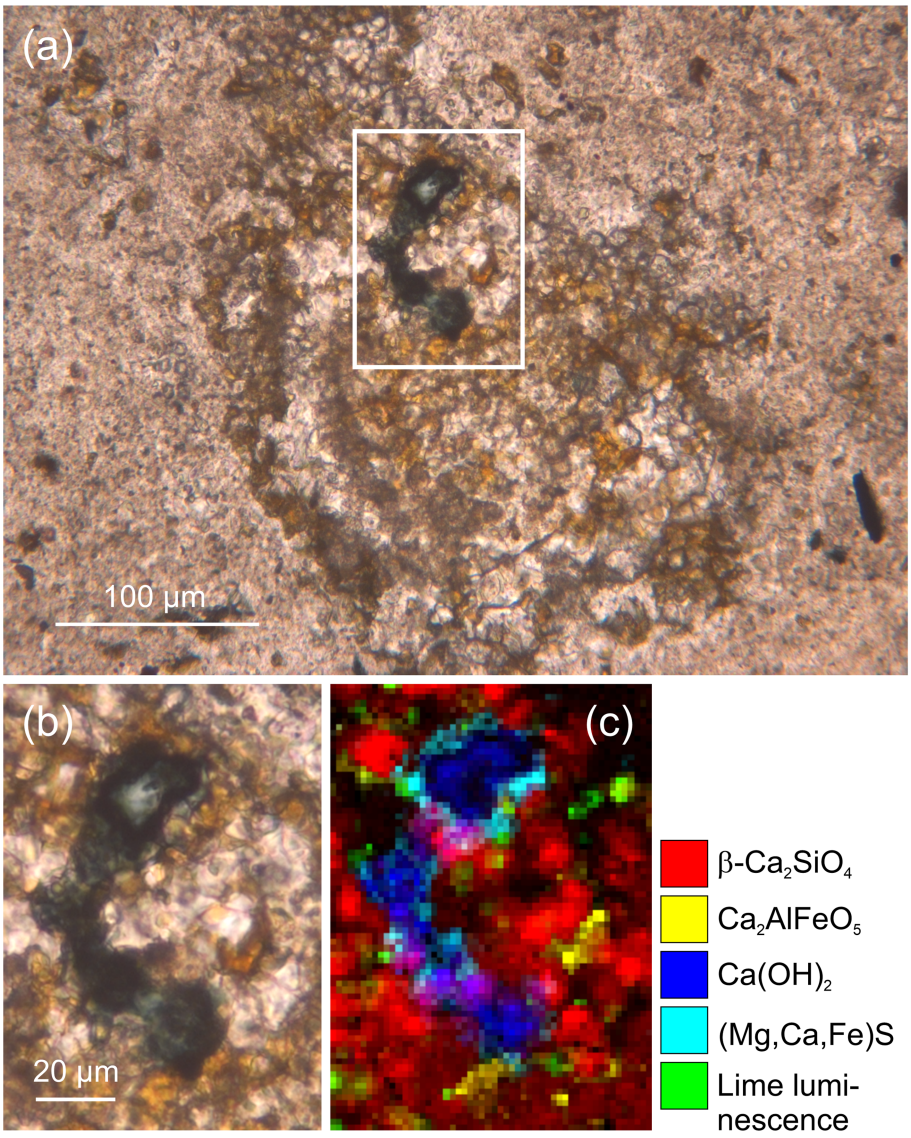

FIGURE 5 Transmitted light micrographs (a, b) and Raman/luminescence map (c) of an unhydrated binder remnant in a meso Portland cement stone [Colour figure can be viewed at wileyonlinelibrary.com]

3.3 | The reason for red lime luminescence

After having understood MgO:Cr^{3+} and similar luminescence emissions, one might think of the integration of Cr^{3+} into the CaO crystal lattice as the cause of the red luminescence of calcium oxide.[1] Figure 4a shows baseline-corrected Raman spectra of hydromagnesite $Mg_5(CO_3)_4(OH)_2{\cdot}4H_2O$, magnesite $MgCO_3$, dolomite $CaMg(CO_3)_2$ and calcite $CaCO_3$ (i.e., the main mineral in a limestone powder) acquired in the range of 200 to 1200 cm^{-1}. Note that some minerals exhibit additional bands outside this range, for example, the carbonate antisymmetric stretching mode at 1436 cm^{-1} of calcite[1] and the OH stretching bands of hydromagnesite shown in Figures 1 and S1. The characteristic Raman shifts, which are in agreement with data from the RRUFF spectral library[19] and with literature data,[16,20,21] allow the clear distinction and identification of these minerals. After calcination at 1100°C, resulting in complete conversion into MgO, CaO or mixtures of both, the luminescence spectra shown in Figure 4b were acquired using the same Raman spectrometer.

The vibrational side bands of the different calcinated mineral or rock samples and of the burnt lime investigated in our predecessor study[1] appear on the same shift positions, that is, the vibrational wavenumbers of MgO mentioned above. Thus, the red luminescence emission observed after calcination of all investigated phases is due to MgO:Cr^{3+}. A comparison of the radii of the involved ions explains the unlikeliness of Ca^{2+} exchange by Cr^{3+} in CaO. With a radius of 62 pm, Cr^{3+} can easily replace Mg^{2+} (72 pm) in MgO and Al^{3+} (54 pm) in Al_2O_3, whereas the discrepancy in size makes impossible the integration of Cr^{3+} into the octahedral site of a Ca^{2+} ion having a radius of 100 pm. With this knowledge, also

the spectrally broad luminescence emission in the yellow-orange range observed in CaO when excited by a green laser[1] can now be explained as due to the $^4T_{2g} \rightarrow {}^4A_{2g}$ transition of MgO:Cr^{3+} mentioned above and described in the literature to appear at around 16 150 cm^{-1}[11] or 619 nm, respectively.

The MgO:Cr^{3+} luminescence emission of calcinated calcium carbonate can be simply explained by traces of magnesium and chromium in the starting material. Note that chromium was not detectable by X-ray fluorescence microanalysis (μXRF) in all four mineral/stone samples, and the magnesium content was around the detection limit in limestone powder (0.03% ± 0.02%), but small trace amounts of these elements might be enough to produce a significant effect in Raman measurements, when taking in mind that fluorescence emission can be several orders of magnitude stronger than Raman scattering. This hypothesis was confirmed by an experiment: heterogeneously distributed luminescence that is locally detectable by Raman microspectroscopy can be triggered even in analytical grade $CaCO_3$ (≥99%; magnesium content specified as ≤0.02%) when mixed with Cr_2O_3 prior to calcination (see Figure S5). This explanation surely holds true for many examples of CaO, in real samples often containing at least traces of its chemical relative MgO, which opens a way to detect these Raman-inactive species in Raman experiments.

The observed increase of the effect as a function of calcination temperature of hydromagnesite mentioned above (see Figure S2) can be explained by temperature-dependent diffusion rates of Cr^{3+} ions into MgO.[22] Interestingly, when burned under the same conditions, trends in the intensities of luminescence features can be observed (see Figures S6 and S7): both the intensities of vibrational side bands relative to the R line and the intensity of the underlying broadband emission decrease as a function of calcination temperature. We also observed partial bleaching of the red broadband emission during laser illumination on a timescale of minutes, indicating that further to the previously assigned $^4T_{2g} \rightarrow {}^4A_{2g}$ emission of rhombic Cr^{3+} centres,[23] this effect might partly be due to luminescing crystal lattice defects or amorphous domains, as recently observed in anhydrite synthesised at different temperatures.[24] Comparison of Figure S6 with Figure 4 demonstrates that these relative intensity variations not only depend on the calcination temperature: the 10-mg powders calcinated at 1100°C in a heating stage for 10 min yield around 1:1 intensity ratios between the R line and the vibrational band at +432 cm^{-1} (see Figure 4b), whereas such ratio relates to 500–600°C in the hydromagnesite experiment performed with 5-g material and 4-h holding time in the laboratory furnace (see Figure S6). Thus, the observed spectral variations might be 'fingerprints' of the whole process, potentially including effects from composition, amount and comminution of the starting material, the calcination temperature as well as heating, holding and cooling times. Further research is needed to study the possible application of this effect as a mineral thermometer.

3.4 | Making use of lime luminescence in materials analysis

Figure 5a shows the transmitted light microscopy image (parallel Nicols) of a thin section of a sample taken from a cast ornament decorating the façade of the residential building Florastrasse 54 in Zurich (Switzerland), in view of phase assemblage and heterogeneity of unhydrated clinker remnants classified as meso Portland cement mortar in a previous study.[2] This early cement type contains significant amounts of free lime CaO because of the composition of the feedstock and its deficient comminution and homogenisation as well as the comparatively low calcination temperatures typically reached in the intermittently operated shaft kilns of the 19th century.[25–27] On the area revealed by the excerpt in Figure 5b, the distributions of the clinker phases present in a residual binder grain have been plotted based on their Raman spectra and the intensities of characteristic marker bands (see Figure 5c), as explained in more detail in Schmid and Dariz[28] and in Section 2.3 (another Raman map acquired on a different region of the same thin section is shown in Figure S8). In short terms, the Raman spectra acquired during the mapping experiments were compared with reference spectra from our own collection[1,2,28,29] and assigned to individual phases (see Figure S9). Baseline-corrected peak heights of characteristic marker bands of phases were plotted in different false colours and overlaid to yield the Raman microspectroscopic images in Figures 5c and S8c. β-Belite (β-Ca_2SiO_4, or β-C_2S in cement chemist's notation) is the dominating calcium silicate clinker phase, because the aforementioned characteristics of the raw feed and the burning regime lead to the absence or only a small content of alite (Ca_3SiO_5 or C_3S, respectively). As previously demonstrated on the basis of Raman band shift evaluation,[29] the stoichiometry of the calcium aluminoferrite phase corresponds to brownmillerite (Ca_2AlFeO_5 or C_4AF, respectively).

The colourless to greenish black, large cluster in the centre of the mapped area was determined to mainly consist of portlandite $Ca(OH)_2$. The Raman spectrum (Figure S9) is in good agreement with the spectrum of highly pure $Ca(OH)_2$ shown in fig. 1 in our predecessor paper[1] and additionally contains a Raman band at

282 cm^{-1} of yet unknown origin (see Figure S10), which was previously found by Dharmaraja Krishnamurti in portlandite prepared by slowly evaporating a saturated $Ca(OH)_2$ solution of unknown purity. Even though coinciding with a crystal lattice vibration of calcite, $CaCO_3$ was correctly excluded as source of this band because of its missing most prominent Raman mode at 1086 cm^{-1} (cf. trace (1) in Figure S10).[30] Krishnamurty confirmed its interpretation as genuinely due to $Ca(OH)_2$ by the detection of its combination bands (sum and difference frequencies) with infrared OH stretch modes.[31]

Some $Ca(OH)_2$ spectra acquired along the border of the portlandite cluster in the Raman maps in Figures 5 and S8 additionally contain a signal at 319 cm^{-1} and a shoulder at 287 cm^{-1} (see trace (2) in Figure S10). These band positions agree with spectra of magnesium–calcium–iron sulphides.[32] As iron(III) sulphide is instable and spontaneously dissociates into iron(II) sulphide and elemental sulphur or is easily converted into FeS by reducing agents, we propose the formula (Mg,Ca,Fe)S. The iron content explains the greenish black colour (cf. the greenish black layer observed in some boiled eggs on the surface of the egg yolk, which is due to the formation of FeS[33]). Already in the 19th century, sulphurous raw materials and solid fuels (coke, charcoal, black or brown coal) were identified as the sulphur source for the observed formation of oldhamite CaS and pyrrhotite/troilite $Fe_{1-x}S$/FeS during clinkering.[34–38] The presence of calcium sulphide and a 'complex iron sulphide' in Portland cement clinker was linked to reducing conditions in the kiln atmosphere by Fritz Gille et al. in 1965.[39] Recently, the burning of pyrite-bearing marlstone and brown coal was found to contribute to the formation of sulphur-bearing cement clinker phases and solid solutions incorporating isolated minute inclusions of the iron sulphide pyrrhotite $Fe_{1-x}S$ and droplets of CaS in 19th-century Austrian natural Portland cement.[40,41]

In contrast to these previously described morphologies of sulphides within cement clinker, we observed extensive layers of greenish black (Mg,Ca,Fe)S covering the relatively highly abundant free lime clusters. Our hypothesis of formation is predicated on the reaction of gaseous H_2S present in (locally) reducing kiln atmosphere with magnesium-containing calcium oxide (magnesium content confirmed by MgO:Cr^{3+} luminescence) and iron compounds, resulting in a layer of chemically stable and water-insoluble (Mg,Ca,Fe)S on the surface of the free lime crystals. The shape of the cluster (and of the $Ca(OH)_2$ shown in fig. 6 in Dariz et al.[2]) is in line with free lime described in the literature to occur in cement clinker as colourless rounded grains, singly or in clusters.[39,42] During preparation of the thin-sectional sample, the clinker remnant enclosing clusters of free lime was cut through; hence, the latter hydrated into portlandite due to exposure to the atmosphere. This hypothesis is confirmed by still intact CaO present within the subsurface of the binder nodule, which can be detected because of its strong lime luminescence emission.[1] Based on the present study, we conclude that the luminescence is due to MgO:Cr^{3+} in CaO, which vanishes at the moment of dissolution of the periclase MgO crystal lattice and conversion into brucite $Mg(OH)_2$, whose Raman spectrum is not detected because of its trace amount.

A comparison of lime luminescence spectra from different spots of this sample yields a homogeneous picture in terms of relative intensities of N lines and vibrational bands (see Figure S11), which differ from the spectroscopic signatures of the MgO:Cr^{3+} synthesised within our experiments (see Figures 2–4, S2, S3, S5 and S6). This might confirm its nature as a 'fingerprint' of raw materials and calcination conditions.

4 | CONCLUSIONS

Whereas our predecessor paper focused on avoiding the misinterpretation of a narrowband red luminescence emission observed in CaO as due to Raman scattering and thus on the correct Raman and luminescence spectra of the phases of the lime cycle,[1] the present article explains the reason for and theoretical background of this lime luminescence, paving the way for its use in materials analysis. We found that the pattern of a sharp central line at 699.1-nm wavelength or 14 304-cm^{-1} absolute wavenumbers, respectively, with almost symmetrically arranged vibrational satellite bands is due to the luminescence emission by MgO:Cr^{3+} present in calcinated calcium, magnesium and Ca–Mg lime phases as major component, minor component or trace. Because the luminescence pattern is as specific as a Raman spectrum, this effect enables access to vibrational data of a Raman-inactive phase and its detection within complex materials by using a Raman microscope, which was successfully demonstrated in the application to a 19th-century meso Portland cement sample. As the shown concept applies to several other mineral phases doped with *d*-block element ions, this study aims to sharpen the awareness of the potential of such luminescence emissions as extension of the possibilities of Raman spectroscopy and microspectroscopy. Therefore, we would like to draw the reader's attention to the according literature, as, for example, the comprehensive review provided by Michael Gaft et al.[43] Further research is needed to clarify whether Cr^{3+}, other *d*-block element ions or further effects are the sources of similar narrowband luminescence patterns observed in lime-based building materials

within the near-infrared spectral range,[13] also taking in mind a luminescence pattern centred at approximately 880 nm observed in a burnt limestone in our predecessor study,[1] which was not reproduced within the spectroscopic analyses presented here.

ACKNOWLEDGEMENTS

We gratefully acknowledge funding of the equipment by Deutsche Forschungsgemeinschaft DFG GSC 1013 SALSA, Museum für Naturkunde Berlin (Dr. Ralf-Thomas Schmitt) for providing the magnesite and dolomite samples, and Philipp Drabetzki, André Gardei and Dr. Sebastian Simon (Bundesanstalt für Materialforschung und -prüfung) for conducting X-ray fluorescence microanalysis (μXRF) of the investigated mineral and stone powders. We furthermore thank Meletta Strebel Architekten AG (Zurich, Switzerland) for the cement stone sample from the façade of the residential building Florastrasse 54 in Zurich.

ORCID

Thomas Schmid https://orcid.org/0000-0001-9708-931X

REFERENCES

[1] T. Schmid, P. Dariz, *J. Raman Spectrosc.* **2015**, *46*, 141.
[2] P. Dariz, J. Neubauer, F. Goetz-Neunhoeffer, T. Schmid, *Eur. J. Mineral.* **2016**, *28*, 907.
[3] O. Deutschbein, *Ann. Phys. (Berlin)* **1932**, *406*, 712.
[4] A. L. Schawlow, *J. Appl. Phys.* **1962**, *33*, 395.
[5] G. F. Imbusch, A. L. Schawlow, A. D. May, S. Sugano, *Phys. Rev.* **1965**, *140*, A830.
[6] A. M. Glass, *J. Chem. Phys.* **1967**, *46*, 2080.
[7] C.-C. Chao, *J. Phys. Chem. Solids* **1971**, *32*, 2517.
[8] A. Chopelas, *Earth Planet. Sci. Lett.* **1992**, *114*, 185.
[9] A. Chopelas, *Phys. Chem. Minerals* **1996**, *23*, 25.
[10] M. Czaja, M. Kądziołka-Gaweł, R. Lisiecki, S. Bodył-Gajowska, Z. Mazurak, *Phys. Chem. Miner.* **2014**, *41*, 115.
[11] J. A. Aramburu, P. García-Fernández, J. M. García-Lastra, M. T. Barriuso, M. Moreno, *J. Phys. Condens. Matter* **2013**, *25*, 175501.
[12] R. S. Krishnan, *Nature* **1947**, *160*, 26.
[13] Z. Kaszowska, K. Malek, E. Staniszewska-Slezak, K. Niedzielska, *Spectrochim. Acta A* **2016**, *169*, 7.
[14] T. Schmid, N. Schäfer, S. Levcenko, T. Rissom, D. Abou-Ras, *Sci. Rep.* **2015**, *5*, 18410.
[15] L. A. Hollingbery, T. R. Hull, *Thermochim. Acta* **2010**, *509*, 1.
[16] R. L. Frost, *J. Raman Spectrosc.* **2011**, *42*, 1690.
[17] T. Schmid, R. Jungnickel, P. Dariz, *J Raman Spectrosc.* **2019**, *50*, 1154.
[18] F. Freund, in *Proton Conductors: Solids, Membranes and Gels—Materials and Devices*, (Ed: P. Colomban), Cambridge University Press, Cambridge **1992** 138.
[19] B. Lafuente, R. T. Downs, H. Yang, N. Stone, in *Highlights in Mineralogical Crystallography*, (Eds: T. Armbruster, R. M. Danisi), W. De Gruyter, Berlin **2015** 1.
[20] P. Gillet, C. Biellmann, B. Reynard, P. McMillan, *Phys. Chem. Minerals* **1993**, *20*, 1.
[21] W. J. B. Dufresne, C. J. Rufledt, C. P. Marshall, *J Raman Spectrosc.* **2018**, *49*, 1999.
[22] R. S. de Biasi, M. L. N. Grillo, *Solid State Commun.* **2004**, *132*, 107.
[23] M. O. Henry, J. P. Larkin, G. F. Imbusch, *Phys. Rev. B* **1976**, *13*, 1893.
[24] T. Schmid, R. Jungnickel, P. Dariz, *Minerals* **2020**, *10*, 115.
[25] A. Francis, *The Cement Industry 1796–1914: A History*, David & Charles Inc., Newton Abbot **1977** 319.
[26] P. Hewlett (Ed), *Lea's Chemistry of Cement and Concrete*, Fourth ed., Butterworth Heinemann, Oxford **2004** 1057.
[27] J. Stark, B. Wicht, *Zement und Kalk*, Birkhäuser, Basel **2000** 376.
[28] T. Schmid, P. Dariz, *Heritage* **2019**, *2*, 1662.
[29] P. Dariz, T. Schmid, *Mater Charact* **2017**, *129*, 9.
[30] D. Krishnamurti, *Proc. Indiana Acad. Sci.* **1959**, *50 A*, 223.
[31] D. Krishnamurti, *Proc. Indiana Acad. Sci.* **1959**, *50 A*, 247.
[32] C. Avril, V. Malavergne, R. Caracas, B. Zanda, B. Reynard, E. Charon, E. Bobocioiu, F. Brunet, S. Borensztajn, S. Pont, M. Tarrida, F. Guyot, *Meteorit. Planet. Sci.* **2013**, *48*, 1415.
[33] C. K. Tinkler, M. Crossland Soar, *Biochem. J.* **1920**, *14*, 114.
[34] W. Michaëlis, *Die hydraulischen Mörtel, insbesondere der Portland-Cement, in chemisch-technischer Beziehung*, Quandt & Händel, Leipzig **1869** 315.
[35] H. Kämmerer, Notizblatt des deutschen Vereins für Fabrikation von Ziegeln, Thonwaaren, Kalk und Cement **1877**, *13*, 304–309.
[36] H. Kämmerer, Notizblatt des deutschen Vereins für Fabrikation von Ziegeln, Thonwaaren, Kalk und Cement **1878**, *14*, 343–351.
[37] G. Feichtinger, *Die chemische Technologie der Mörtelmaterialien*, Friedrich Vieweg und Sohn, Braunschweig **1885**, 478.
[38] A. Tarnawski, *Kalk, Gyps, Cementkalk und Portland-Cement in Österreich-Ungarn*, Rudolf Brzezowsky & Söhne, Wien **1887**.
[39] F. Gille, I. Dreizler, K. Grade, H. Krämer, E. Woermann, *Mikroskopie des Zementklinkers*, Beton-Verlag, Düsseldorf **1965** 75.
[40] F. Pintér, C. Gosselin, *Cem. Concr. Res.* **2018**, *110*, 1.
[41] F. Pintér, C. Gosselin, T. Köberle, I. Vidovszky, J. Weber, *Proceedings of the 5th Historic Mortars Conference*, RILEM Publications, Paris **2019**, 819.
[42] D. Campbell, *Microscopical Examination and Interpretation of Portland Cement and Clinker*, Second ed., Portland Cement Association, Skokie **1999** 201.
[43] M. Gaft, R. Reisfeld, G. Panczer, *Modern Luminescence Spectroscopy of Minerals and Materials*, Second ed., Springer International Publishing, Basel **2015**.

SUPPORTING INFORMATION

Additional supporting information may be found online in the Supporting Information section at the end of this article.

How to cite this article: Schmid T, Kraft R, Dariz P. Shedding light onto the spectra of lime—Part 2: Raman spectra of Ca and Mg carbonates and the role of *d*-block element luminescence. *J Raman Spectrosc*. 2021;52:1462–1472. https://doi.org/10.1002/jrs.6174